7 Circumstellar envelopes of AGB stars

The extensive mass loss of AGB stars makes that they are surrounded by an extended circumstellar envelope (CSE), the maximum radius of which can be estimated as

$$r_{\rm CSE} = t_{\rm AGB} v_\infty \simeq 10^6 {\rm yr} \times 10 {\rm kms}^{-1} \sim 10^{19} {\rm cm} \tag{69}$$

This is a maximum value since the wind material will start to mix with the ISM at very large radii, and it also assumes that there is no velocity difference between the star and the interstellar gas. In addition the density drops with radius r in the expanding CSE (as r^{-2} for a constant mass loss rate $\dot{M}$ and velocity v_∞), so the outermost parts are too low density to be observable. Using some typical numbers we can estimate the density as

$$n(r) = \frac{\dot{M}}{4\pi \mu m_{\rm H} v_\infty r^2} \simeq 10^6 \left[\frac{\dot{M}}{10^{-5} M_\odot {\rm yr}^{-1}}\right] \left[\frac{15 {\rm kms}^{-1}}{v_\infty}\right] \left[\frac{10^{15} {\rm cm}}{r}\right]^2 \quad {\rm cm}^{-3} \tag{70}$$

For comparison, the canonical value for the density of the ISM is 1 $\rm cm^{-1}$
As we saw above, dynamically all of the interesting action is quite close to the star, where the wind in launched and the mass loss rate is determined. However, the outer layers of the CSE show chemically interesting processes, and are of because of their size and lower optical depth, easier to observe.

7.1 Temperatures

The temperature of the CSE is a function of radius, and is set by the heating and cooling rates. Since the heating and cooling processes are different for the gas and the dust, their temperatures will generally be different.
Even in the absence of heating and cooling the gas temperature will drop as the CSE material is flowing away from the star. The reason is sometimes called ‘adiabatic cooling’, and is simply caused by the fact that the same energy density has to fill a larger volume as the CSE is expanding. Assuming that the density drops as r^{-2}, as is the case for a stellar wind of constant mass loss rate and in which the velocity is close to v_∞, and taking the adiabatic relation between pressure and density, $p \propto \rho^\gamma$, together with the ideal gas law $p \propto \rho T$, immediately shows that for adiabatic expansion, $T \propto r^{-2(\gamma-1)}$, or $T \propto r^{-4/3}$ for $\gamma = 5/3$.
However, heating and cooling does occur. The main cooling process is radiative cooling from molecular lines, dominated by H_2O and CO around M-stars, and by CO and HCN around C-stars. The main heating process is collisions with dust grains. As we saw, there is generally a velocity difference $v_{\rm drag}$ between the gas and the dust, so upon a collision a certain amount of kinetic energy is transferred to the gas particle. Detailed calculations of these processes show that a typcal radial temperature profile goes as

$$T_{\rm gas}(r) \approx 400 \left(\frac{10^{15} {\rm cm}}{r}\right)^{0.9} \tag{71}$$

The dust temperature is set by the absorption and emission properties of the dust grain. The heating process is the absorption of radiation from the star (at short wavelengths),

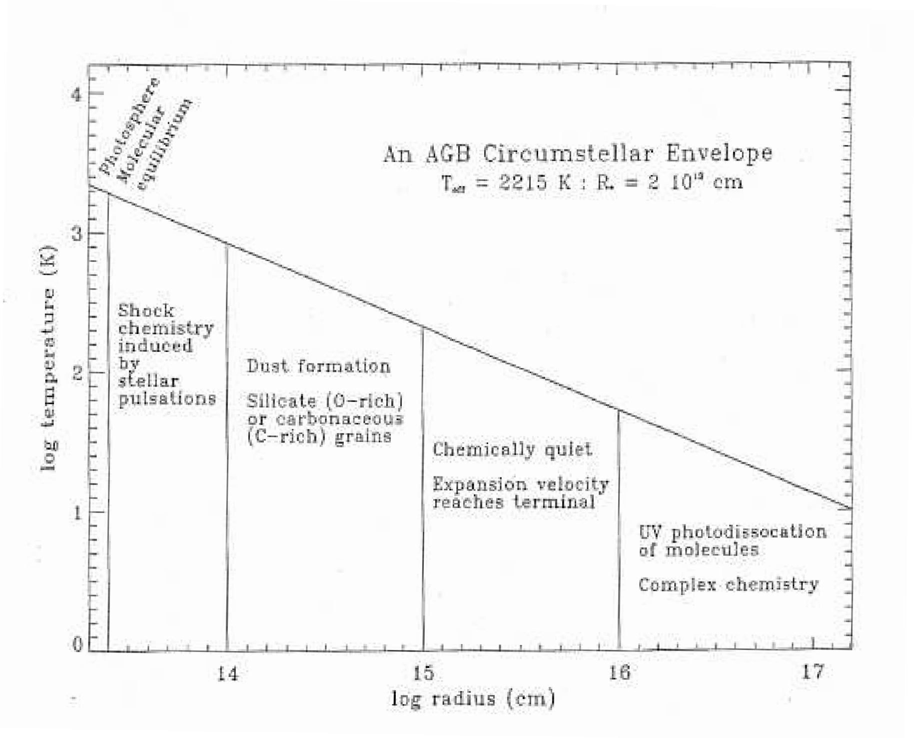

Figure 31: Schematic chemical structure in an AGB CSE. From Marwick (2000)

the cooling process is the emission of thermal radiation from the warm grain (at longer wavelengths). To some extent the problem is not dissimilar to that of deriving the temperature of a planetary surface. It is important to realize that the dust grains neither absorb as a perfect black body (i.e. their absorption coefficient is frequency-dependent), nor emit as one. Balancing the heating and cooling rates gives a radial dependence of the dust temperature

$$T_{\rm dust}(r) \approx T_{\rm eff} \left(\frac{R_*}{2r} \right)^{\frac{2}{4+s}} \tag{72}$$

where an black body spectrum for the star was assumed. The parameter s comes from the frequency dependence of the absorption/emission coefficient ($\propto \nu^s$). Observations suggest that $s \approx 1$.

From the expression above we see that the dust is generally warmer than the gas, but that the temperatures in the CSE are low. The fact that the dust temperature drops for larger distances means that the thermal emission from dust will peak at higher frequencies for the inner parts of the CSE. Observations of the dust continuum at different frequencies will therefore show different parts of the CSE.

7.2 Chemistry

A chemical picture of an AGB CSE looks more or less like this (see Fig. 31):

1. Photosphere: LTE chemistry
2. Pulsating stellar envelope: shock chemistry
3. Dust formation zone
4. Chemically quiet
5. Interstellar UV radiation: photo-dissociation chemistry

Starting at the photosphere, the local high densities produce an equilibrium chemistry with the dichotomy between the case of O-rich and C-rich stars

C $>$ O C-chemistry (C_2H_2, Polycyclic Aromatic Hydrocarbons (PAHs), ...)

C $<$ O O-chemistry (H_2O, SiO, ...)

The reason for this is the stability of the CO molecule, which forms abundantly in both cases, and thus captures all of the C in the O-rich case, and all the O in the C-rich case. The photospheric temperature ($\sim$ 2000 K) is already low enough for molecules to form.

The shocks driven into the outer stellar atmosphere by the stellar pulsations push the chemistry away from LTE. This is the explanation for the 'unusual' molecular abundances found from observations (e.g. increased abundances for SiO, SiS, CS, decreased abundances for NH_3 and CH_4).

In the dust formation zone the so-called refractory elements are removed from the gas phase (Fe, Si, Mg, ...) and end up in dust grains. At the same time the newly formed dust will also become the site of specific chemical reactions which occur much more efficiently on dust surfaces (‘surficide reactions’). As the temperature drops, some molecules may also start to condense out on grain surfaces, for example H_2O, leading to the formation of ice mantles around dust grains.

Beyond radii of $\sim 10^{16}$ cm the gas density has dropped so much that interstellar UV photons can penetrate and start to destroy molecules, a process known as photo-dissociation. This release chemically active radicals and ionized molecules in the gas phase, starting a range of interesting chemical reactions. One of the most abundant radicals is OH, which is the photo-dissociation product of H_2O. The most abundant molecules, H_2 and CO are self-shielding and survive to large radii.

Detailed modelling with chemical networks can give a good idea of the chemical richness of AGB CSEs, see Table. 1

7.3 Observational aspects of CSEs

Many molecules have transitions at millimeter and sub-millimeter wavelengths, see Table 2, and this wavelength range is therefore one of the most interesting ones for studying the CSEs. This type of high frequency radio emission is observed with dishes (SEST, APEX, IRAM). With single dish telescopes it is difficult to achieve high spatial resolution. Still, because these envelopes are expanding, good spectral resolution can partly compensate for the lack of spatial resolution, and single dish observations are commonly used. Figure 32 shows how line shapes can be used to derive information about the optical thickness of the line, the expansion velocity of the CSE, and the size of the emitting region.

The use of an interferometer considerably improves the spatial resolution, and allows one to obtain more detailed images. Actually, since one retains also the velocity information, one obtains ‘image cubes’: images at various frequencies. Figures. 33 and 34 show examples of interferometer observations of the C-stars IRC+10216 and TT Cyg. The observations of IRC+10216 show how different molecular lines trace different parts of the CSE, whereas the circular ring of CO emission around TT Cyg highlights the fact that there are mass loss variations. These observations were both made with the IRAM interferometer. The construction of the ALMA interferometer facility in Chile will considerably improve our imaging capabilities for AGB CSEs, both in spatial and velocity resolution, as well as sensitivity. This is expected to have a large impact on the field.

At infrared wavelengths (best observed from space, for example with IRAS, ISO and Spitzer) both molecules (Table 3) and dust features (Table 4) dominate. The most pronounced dust feature is the 10 μm (or more accurately 9.7μm) Si-feature. Note that not all features have been identified with absolute certainty. The fact that they are rather broad complicates accurate identification.

7.4 Maser emission

The CSEs of AGB stars also often show the phenomenon of natural maser emission. This arises through a combination of a non-LTE distribution of the electrons over the energy levels, combined with stimulated emission. To achieve a non-LTE distribution

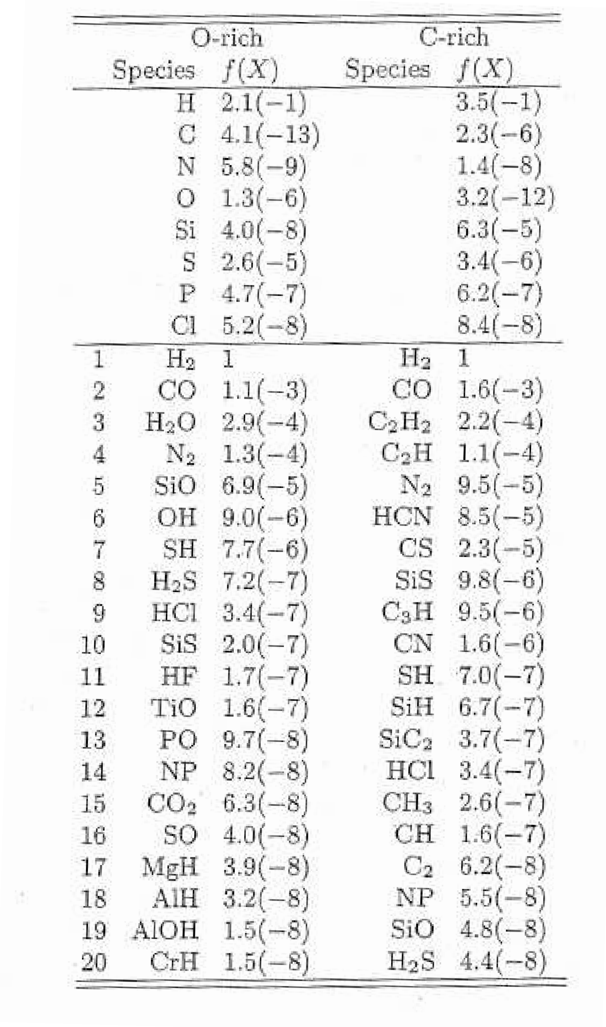

	O-rich		C-rich	
	Species	$f(X)$	Species	$f(X)$
	H	2.1(−1)		3.5(−1)
	C	4.1(−13)		2.3(−6)
	N	5.8(−9)		1.4(−8)
	O	1.3(−6)		3.2(−12)
	Si	4.0(−8)		6.3(−5)
	S	2.6(−5)		3.4(−6)
	P	4.7(−7)		6.2(−7)
	Cl	5.2(−8)		8.4(−8)
1	H_2	1	H_2	1
2	CO	1.1(−3)	CO	1.6(−3)
3	H_2O	2.9(−4)	C_2H_2	2.2(−4)
4	N_2	1.3(−4)	C_2H	1.1(−4)
5	SiO	6.9(−5)	N_2	9.5(−5)
6	OH	9.0(−6)	HCN	8.5(−5)
7	SH	7.7(−6)	CS	2.3(−5)
8	H_2S	7.2(−7)	SiS	9.8(−6)
9	HCl	3.4(−7)	C_3H	9.5(−6)
10	SiS	2.0(−7)	CN	1.6(−6)
11	HF	1.7(−7)	SH	7.0(−7)
12	TiO	1.6(−7)	SiH	6.7(−7)
13	PO	9.7(−8)	SiC_2	3.7(−7)
14	NP	8.2(−8)	HCl	3.4(−7)
15	CO_2	6.3(−8)	CH_3	2.6(−7)
16	SO	4.0(−8)	CH	1.6(−7)
17	MgH	3.9(−8)	C_2	6.2(−8)
18	AlH	3.2(−8)	NP	5.5(−8)
19	AlOH	1.5(−8)	SiO	4.8(−8)
20	CrH	1.5(−8)	H_2S	4.4(−8)

Table 1: The atoms and top 20 molecules produced in LTE calculations for an O-rich star (R Cas with C/O=0.75 and $T_{\rm eff} = 2215$ K) and a C-rich star (IRC+10216 with C/O=1.5 and $T_{\rm eff} = 2300$ K). In both cases the pressure was chosen to be 1.033×10^{-3} atm, corresponding to a total hydrogen density of 3×10^{15} cm^{-3}. $f(X)$ is the fractional abundance of species X relative to H_2 ($k(l) = k \times 10^{l}$). From Millar (2004)

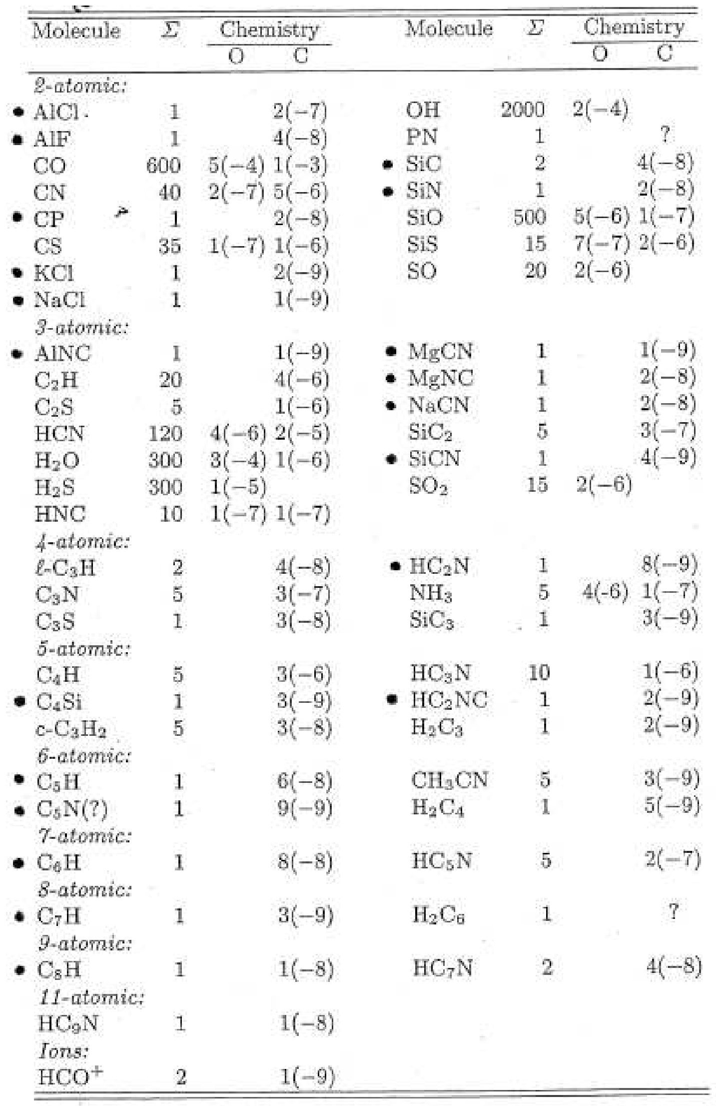

Molecule	Σ	Chemistry		Molecule	Σ	Chemistry	
		O	C			O	C
2-atomic:							
● AlCl	1		2(−7)	OH	2000	2(−4)	
● AlF	1		4(−8)	PN	1		?
CO	600	5(−4)	1(−3)	● SiC	2		4(−8)
CN	40	2(−7)	5(−6)	● SiN	1		2(−8)
● CP	1		2(−8)	SiO	500	5(−6)	1(−7)
CS	35	1(−7)	1(−6)	SiS	15	7(−7)	2(−6)
● KCl	1		2(−9)	SO	20	2(−6)	
● NaCl	1		1(−9)				
3-atomic:							
● AlNC	1		1(−9)	● MgCN	1		1(−9)
C_2H	20		4(−6)	● MgNC	1		2(−8)
C_2S	5		1(−6)	● NaCN	1		2(−8)
HCN	120	4(−6)	2(−5)	SiC_2	5		3(−7)
H_2O	300	3(−4)	1(−6)	● SiCN	1		4(−9)
H_2S	300	1(−5)		SO_2	15	2(−6)	
HNC	10	1(−7)	1(−7)				
4-atomic:							
ℓ-C_3H	2		4(−8)	● HC_2N	1		8(−9)
C_3N	5		3(−7)	NH_3	5	4(-6)	1(−7)
C_3S	1		3(−8)	SiC_3	1		3(−9)
5-atomic:							
C_4H	5		3(−6)	HC_3N	10		1(−6)
● C_4Si	1		3(−9)	● HC_2NC	1		2(−9)
c-C_3H_2	5		3(−8)	H_2C_3	1		2(−9)
6-atomic:							
● C_5H	1		6(−8)	CH_3CN	5		3(−9)
● C_5N(?)	1		9(−9)	H_2C_4	1		5(−9)
7-atomic:							
● C_6H	1		8(−8)	HC_5N	5		2(−7)
8-atomic:							
● C_7H	1		3(−9)	H_2C_6	1		?
9-atomic:							
● C_8H	1		1(−8)	HC_7N	2		4(−8)
11-atomic:							
HC_9N	1		1(−8)				
Ions:							
HCO^+	2		1(−9)				

Table 2: Molecules detected in AGB CSEs at radio wavelengths. The (rough) number of sources detected in each species is given (Σ), as well as abundances with respect to H_2 (O: C/O<1; C:C/O>1; $k(l) = k \times 10^l$). From Olofsson (2004).

.

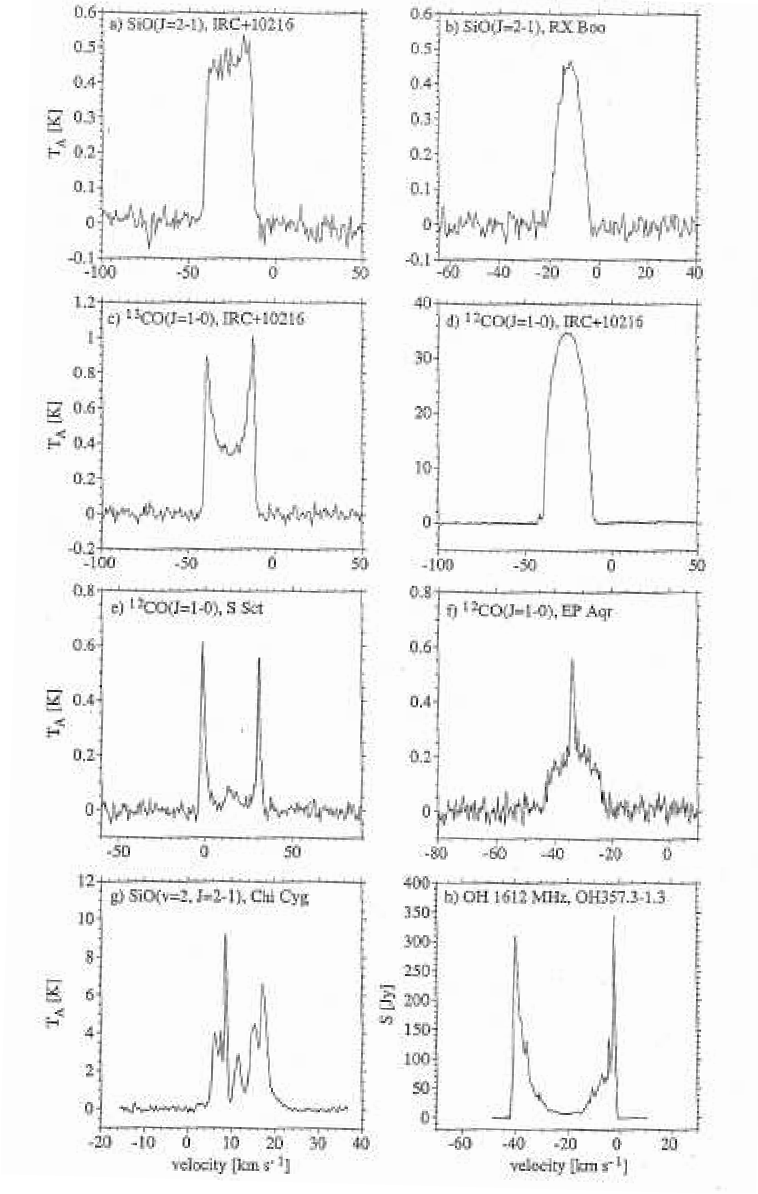

Figure 32: Observed line profiles toward AGB CSEs: (a) optically thin, spatially unresolved emission, (b) optically think, spatially unresolved emission, (c) optically thin, spatially resolved emission, (d) optically thick, spatially resolved emission, (e) emission from geometrically thin, spatially resolved shell, (f) double-component line profile, (g) and (h) maser emission-line profiles. From Olofsson (2004).

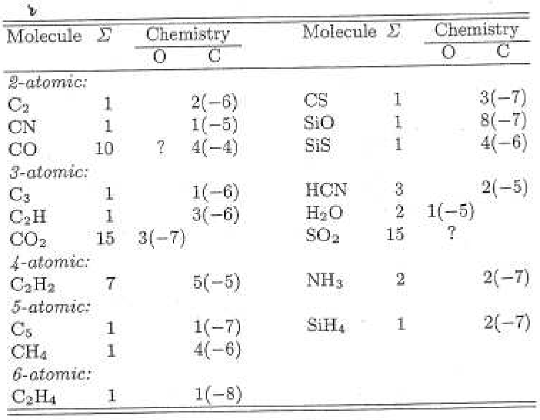

Molecule	Σ	Chemistry		Molecule	Σ	Chemistry	
		O	C			O	C
2-atomic:							
C_2	1		2(−6)	CS	1		3(−7)
CN	1		1(−5)	SiO	1		8(−7)
CO	10	?	4(−4)	SiS	1		4(−6)
3-atomic:							
C_3	1		1(−6)	HCN	3		2(−5)
C_2H	1		3(−6)	H_2O	2	1(−5)	
CO_2	15	3(−7)		SO_2	15	?	
4-atomic:							
C_2H_2	7		5(−5)	NH_3	2		2(−7)
5-atomic:							
C_5	1		1(−7)	SiH_4	1		2(−7)
CH_4	1		4(−6)				
6-atomic:							
C_2H_4	1		1(−8)				

Table 3: Molecules detected in AGB CSEs at infrared and optical wavelengths. The (rough) number of sources detected in each species is given (Σ), as well as abundances with respect to H_2 (O: C/O<1; C:C/O>1; ,$k(l) = k \times 10^l$). From Olofsson (2004).

.

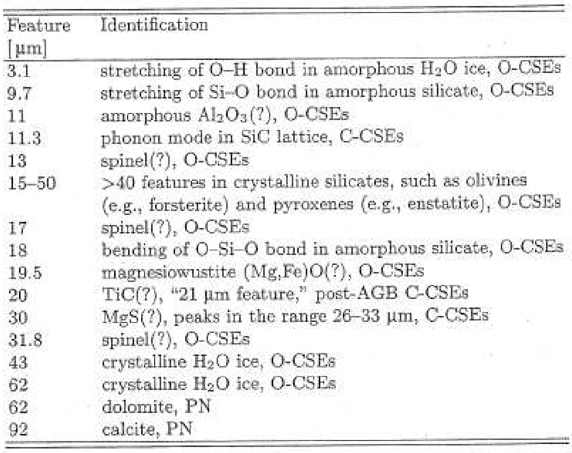

Feature [µm]	Identification
3.1	stretching of O–H bond in amorphous H_2O ice, O-CSEs
9.7	stretching of Si–O bond in amorphous silicate, O-CSEs
11	amorphous Al_2O_3(?), O-CSEs
11.3	phonon mode in SiC lattice, C-CSEs
13	spinel(?), O-CSEs
15–50	>40 features in crystalline silicates, such as olivines (e.g., forsterite) and pyroxenes (e.g., enstatite), O-CSEs
17	spinel(?), O-CSEs
18	bending of O–Si–O bond in amorphous silicate, O-CSEs
19.5	magnesiowustite (Mg,Fe)O(?), O-CSEs
20	TiC(?), "21 µm feature," post-AGB C-CSEs
30	MgS(?), peaks in the range 26–33 µm, C-CSEs
31.8	spinel(?), O-CSEs
43	crystalline H_2O ice, O-CSEs
62	crystalline H_2O ice, O-CSEs
62	dolomite, PN
92	calcite, PN

Table 4: Dust spectral signatures in AGB CSEs. From Olofsson (2004).

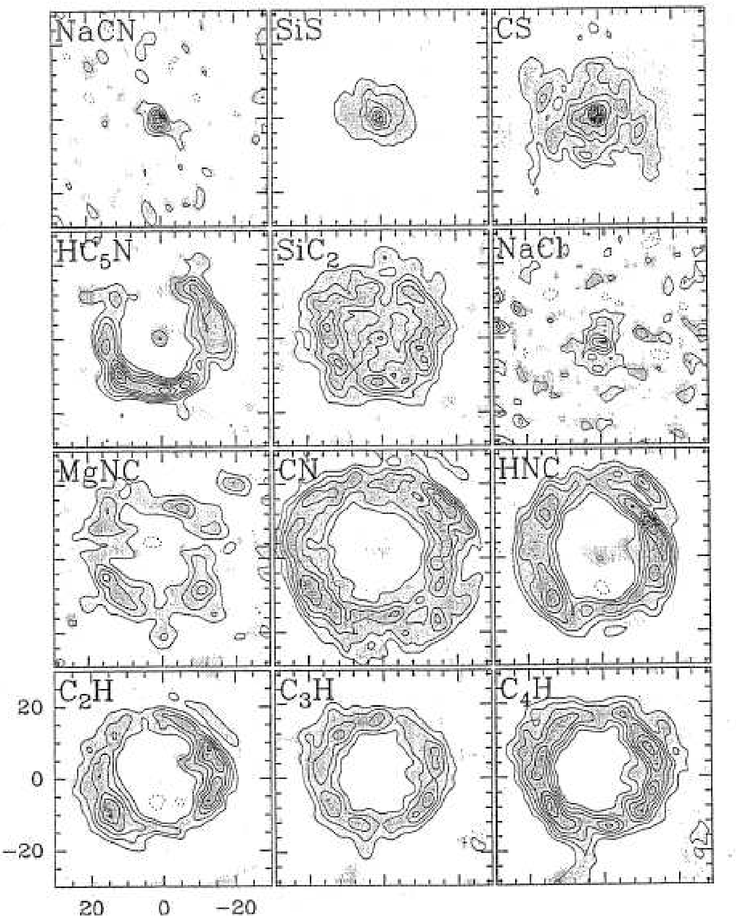

Figure 33: Molecular line brightness, in a narrow velocity interval centered on the systemic velocity, observed towards IRC+10216 (IRAM PdB interferometer; arcsec scale). The observed lines all lie around 100 GHz. From Guélin et al. (1996).

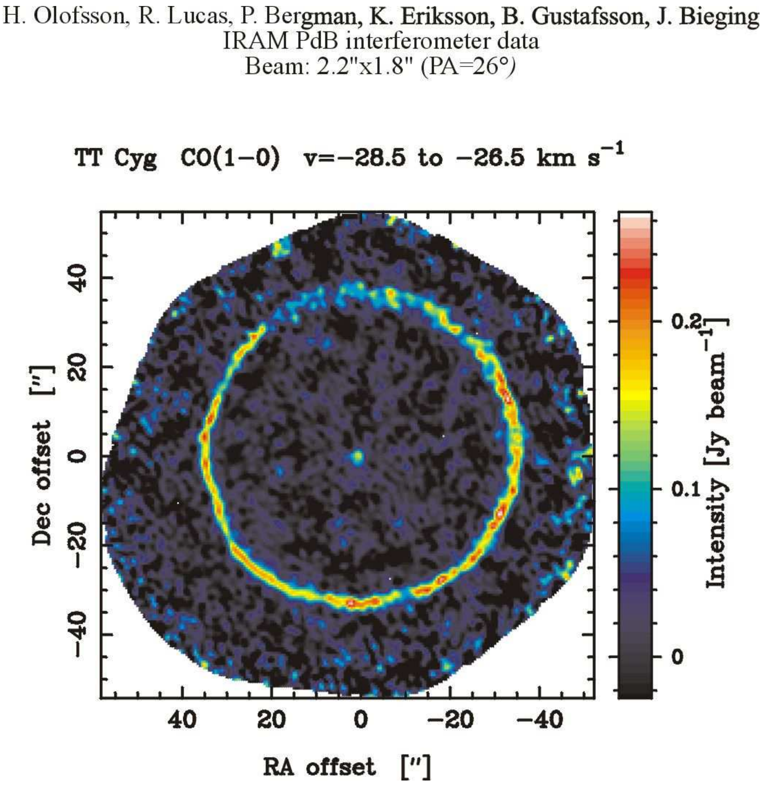

Figure 34: A CO(J=1→0) map of the carbon star TT Cyg in a narrow velocity interval centered at the systemic velocity (IRAM PdB interferometer). The brightness is well fitted by a circular ring of diameter 68″. The emission near to star is from current mass loss, the ring points to an earlier episode of increased mass loss.

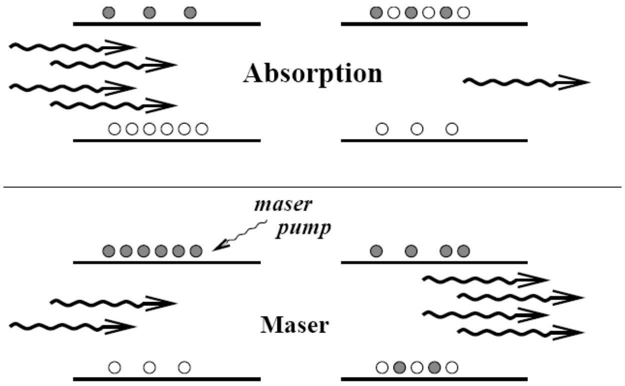

Figure 35: The maser principle. The circles are the electron populations of the two energy levels drawn. Normally, radiation is absorbed by molecules (upper panel) and as a result, the upper population temporarily increases. The absorbed radiation is later emitted at the same frequency. In the maser, a masing molecule is excited into a higher energy level by a pump. Instead of absorbing radiation, the electrons at the upper level are now stimulated by incident radiation to decay to the lower energy level, which results in the emission of photons at the same frequency as the radiation travelling through the maser (lower panel). Consequently, the maser amplifies the radiation of one specific frequency exponentially while the radiation propagates through the masing medium.

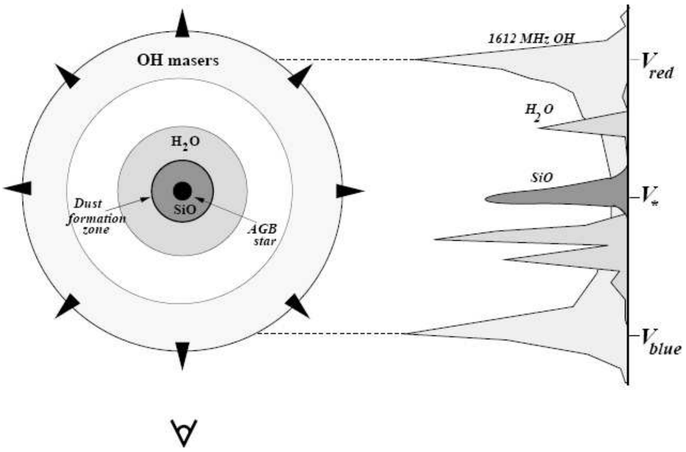

Figure 36: A schematic overview of the masers in a circumstellar envelope and their corresponding spectra. The two peaks in the OH spectrum correspond to the front- and back-side of the expanding envelope. The H_2O masers are found closer to the star and show much more irregular spectra. The SiO masers are found closest to the star and have a velocity closely centered on the stellar velocity.

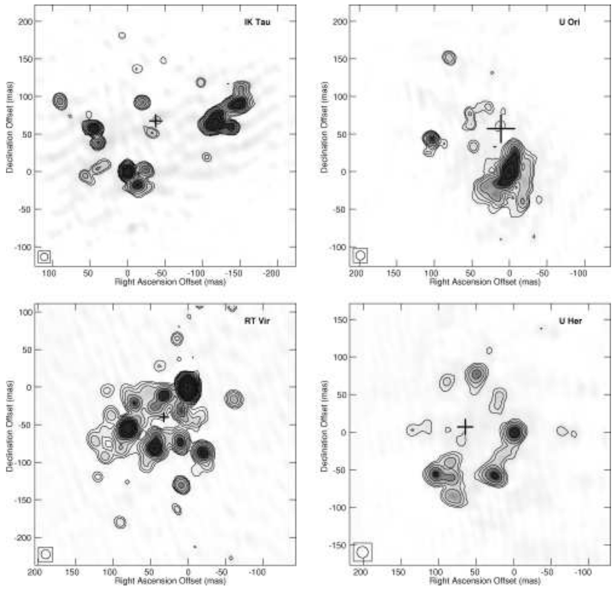

Figure 37: Images of H_2O masers around four different AGB stars. The maser action occurs in spots, but around a clearly defined radius. From ???

one needs a so-called ‘pump’, which can be either radiative or collisional. The stimulated emission process then produces a cascade of photons.

Since stimulated emission is proportional to the local intensity, it enters the equation of radiative transfer as a negative form of absorption. This directly translates into a *negative* optical depth

$$I_\nu = I_{\rm bg} + S_\nu \left(e^{-\tau_\nu} - 1 \right) \tag{73}$$

which means that the intensity grows exponentially and can reach very large values. This makes masers interesting observationally since they can be observed from large distances.

The intensity is limited by the rate at which the level population can be pumped. If the stimulated emission de-excites faster than the pump can restore the non-LTE distribution, the maser is said to ‘saturate’. A small velocity gradient is also needed.

The types of masering molecules found around AGB stars are

SiO masers Inside the dust formation zone $\sim 10^{14}$ cm

H_2O masers Outside the dust formation zone $\sim 10^{15}$ cm

OH masers In the photo-dissociation zone $\sim 10^{17}$ cm

These three types thus provide us with a good sampling of the most important regions of the CSE.

The SiO and H_2O masers mostly show individual ‘spots’ or lumps, wheread the OH maser emission often takes the shape of a thin round shell. In spectra the OH maser line shows a very characteristic two peak shape (coming from the front- and the backside of the maser shell) at a frequency of 1612 MHz. This frequency makes it accessible to most ‘classical’ radio telescopes (such as the VLA and the WSRT), and also to the VLBI networks (giving spatial resolution in the μas range). The stars showing this OH maser emission very often are completely obscured in the optical, and are therefore known as OH-IR stars. They represent a class of O-rich AGB stars with the highest mass loss rates, and the large amount of dust formed inhibits the escape of optical emission.

The pump for the OH maser is infrared emission from the star. Since these stars are variable (with periods of several years), the maser emission also varies, but with a slight delay because of the light travel time across the CSE. The typical radius for OH maser emission is 10^{17} cm, corresponding to a light travel time of a month or so. If we can observe both the front- and backside of the shell, there will be a phase difference between their variability, corresponding to $2R_{\rm OH}/c$. If the angular size of the OH maser shell can be measured, this gives us a direct measurement of the distance to us.

Because of the very non-linear emission mechanism it is hard to use maser data for determining the density structure of CSEs of AGB stars (including their geometry), but they can be excellently used for several other things

- Distance determinations
- High precision astrometry (proper motions and parallaxes).
- Magnetic field estimates.